



Ambient molecular imaging by laser ablation electrospray ionization mass spectrometry with ion mobility separation



Hang Li^a, Brian K. Smith^a, László Márk^b, Peter Nemes^a, Javad Nazarian^{c,d}, Akos Vertes^{a,*}

^a Department of Chemistry, W. M. Keck Institute for Proteomics Technology and Applications, The George Washington University, 725 21st Street, N.W., Washington, DC 20052, USA

^b Department of Analytical Biochemistry, Institute of Biochemistry and Medical Chemistry, Janos Szentagothai Research Center, MTA-PTE Human Reproductive Research Group, University of Pécs, H-7624 Pécs, Hungary

^c Research Center for Genetic Medicine, Children's National Medical Center, Washington, DC 20010, USA

^d Department of Integrative Systems Biology, George Washington University, School of Medicine and Health Sciences, Washington, DC 20052, USA

ARTICLE INFO

Article history:

Received 29 March 2014

Received in revised form 21 June 2014

Accepted 27 June 2014

Available online 28 June 2014

Keywords:

Laser ablation electrospray ionization

LAESI

Ambient ionization

Ion mobility separation

Mass spectrometry imaging

ABSTRACT

Mass spectrometry imaging (MSI) by laser ablation electrospray ionization (LAESI) enables the lateral mapping of molecular distributions in untreated biological tissues. However, direct sampling and ionization by LAESI–MSI limits the differentiation of isobaric ions (e.g., structural isomers) in a complex sample. Ion mobility separation (IMS) of LAESI-generated species is sufficiently fast to be integrated with the MSI experiments. Here, we present an imaging technique based on a novel combination of LAESI–MSI with IMS that enables *in vivo* and *in situ* imaging with enhanced coverage for small metabolites. Ionized molecules produced at each pixel on the tissue were separated by a traveling wave IMS and analyzed by a high performance quadrupole time-of-flight mass spectrometer. Plant (*Pelargonium peltatum* leaves) and animal tissues (frozen mouse brain sections) were imaged under atmospheric pressure. In LAESI–IMS–MSI, a multidimensional dataset of *m/z*, drift time (DT), ion intensity, and spatial coordinates was collected. Molecular images for the *P. peltatum* leaf illustrated that the distributions of flavonoid glycoside ions are aligned with a vein pattern in the tissue. Differentiation of isobaric ions over DT reduced the chemical interferences and allowed separate imaging of these ions. Molecular images were constructed for selected ions in the sagittal sections of the mouse brain, and isobaric species were distinguished by differences in drift times corresponding to distinct molecular structures or conformations. We demonstrated that IMS enhanced the metabolite coverage of LAESI in biological tissues and provided new perspective on MSI for isobaric species.

© 2014 Elsevier B.V. All rights reserved.

1. Introduction

Mass spectrometry imaging (MSI) has emerged as an important tool to visualize the spatial distributions of multiple molecules across sample surfaces. Various ionization techniques have been implemented for molecular imaging of biological specimens [1–5]. Secondary ion mass spectrometry (SIMS) [6] and matrix-assisted laser desorption ionization (MALDI) [7] mass spectrometry (MS) are the most widely used MSI methods, both of which require vacuum conditions. SIMS has demonstrated advantages in imaging of inorganic compounds at relatively low masses with very high resolution (~100 nm) [1], whereas MALDI-MS excels in

imaging of large molecules, particularly proteins, with a typical spatial resolution of tens of microns [8,9]. In the past decade, the implementation of ambient ionization techniques for MSI has grown rapidly, enabling operation under native conditions with minimum or no sample preparation [1]. With the advent of ambient ionization sources, such as desorption electrospray ionization (DESI) [10–13], laser ablation electrospray ionization (LAESI) [14–16], desorption atmospheric pressure photoionization (DAPPI) [17], probe electrospray ionization (PESI) [18], and nanospray desorption electrospray ionization (nanoDESI) [19,20], *in vivo* and *in situ* MSI have become accessible. Ambient MSI facilitates the simultaneous imaging of small metabolites, lipids, polypeptides, and large proteins in biological samples. In most of these techniques, soft ionization yields minimum or no fragmentation, due to their relatively low energy deposition [21]. Ambient MSI has been extensively applied in tissue analysis,

* Corresponding author. Tel.: +1 202 994 2717; fax: +1 202 994 5873.
E-mail address: vertes@gwu.edu (A. Vertes).

including drug development [22], forensic sciences [23], clinical research, and biomarker discovery [1].

Designed to utilize the natural water content of cells and tissues as a matrix, LAESI uses mid-IR laser pulses at 2940 nm to excite the O–H vibrations in the sample for efficient energy deposition [14]. Sudden energy deposition leads to ablation, driven by phase explosion and ejection of particulates by the recoil pressure [24,25]. The ablated particles are captured by the electrospray, and sample-related ions are produced. Two-dimensional LAESI-MSI has been demonstrated for the mapping of metabolite and lipid distributions in live plants and frozen rat brain sections [15,26]. The feasibility of three-dimensional LAESI-MSI has also been shown for plant leaves with a depth resolution of $\sim 30 \mu\text{m}$ [16]. The obtained molecular images exhibit good correlation with visually observed features (e.g., variegation pattern) and known biological functions (e.g., localization of chlorophyll).

As a direct ionization technique, conventional LAESI-MS lacks a separation step, known to improve molecular coverage for bioanalytical methods. Likewise, direct ionization exhibits an inherent limitation in the imaging of, for example, isobaric compounds in complex samples. In conventional LAESI-MS, a number of ions, especially isobaric or isomeric structures, may interfere with each other resulting in distorted molecular images [27,28]. For example, lipids often interfere with multiply charged peptides in the m/z 600–1200 range [29]. Therefore, it seems beneficial to integrate an on-line separation step with LAESI-MSI.

Ion mobility spectrometry was first introduced in the early 1970s [30]. Gas phase ions are separated based on their differences in collision cross sections by driving them through a buffer gas using electric fields [27,29,31,32]. Different from traditional separation methods, e.g., liquid chromatography, capillary electrophoresis, and gel-based separations, that take place on the time scale of many minutes [28], IMS is sufficiently rapid (separation takes typically less than 1 s) to be coupled with direct ionization, MS and MSI experiments. It had been combined with MALDI-MSI under vacuum conditions and was demonstrated for the imaging of biological samples [29,32–39]. The combination of

IMS with MS enables a multi-dimensional gas phase separation, based on the mass, charge states, and molecular structures [29].

Here we present an IMS-MSI technique by integrating it with a LAESI ion source that enables *in vivo* and *in situ* investigations under ambient conditions. For imaging, ions generated by LAESI from the tissue at multiple locations are separated by IMS within milliseconds according to their molecular structures and conformations. The separated ions are analyzed by a quadrupole time-of-flight (Q-TOF) mass spectrometer for identification. Distribution of metabolites, lipids, and polypeptides represented by m/z combined with drift time (DT) are mapped across the tissue surface.

2. Materials and methods

2.1. LAESI-IMS-MSI

Imaging experiments were performed by LAESI-IMS-MS using a high performance quadrupole time-of-flight (Q-TOF) mass spectrometer (Synapt G2 S, Waters Co., Milford, MA, USA) equipped with a home-built LAESI ionization source, and a programmable xyz-translation stage. In the LAESI event, Q-switched 5 ns mid-IR laser pulses at 2940 nm wavelength (IR Opolette 100, Optronic Inc., Carlsbad, CA, USA) were focused by a single plano-convex lens (Infrared Optical Products, Farmingdale, NY, USA) onto the sample surface to produce an ablation plume. The diameter of the focal spot was $\sim 150 \mu\text{m}$. Particles from the generated plume combined with the charged droplets in an electrospray. A spray solution of 50% methanol with 0.1% acetic acid (v/v) was used for positive ion mode analysis. A syringe pump supplied this solution at a flow rate of $0.3 \mu\text{L}/\text{min}$ to a metal capillary (MT320-50-5-5, New Objective, Woburn, MA, USA) held at 3100 V to produce a stable electrospray. The ions generated by LAESI entered the traveling wave ion guide of the mass spectrometer through an orifice. Ions were initially confined to a traveling wave trap where, if needed for structural identification, collision-induced dissociation could be performed. They were then released into a traveling wave drift tube for

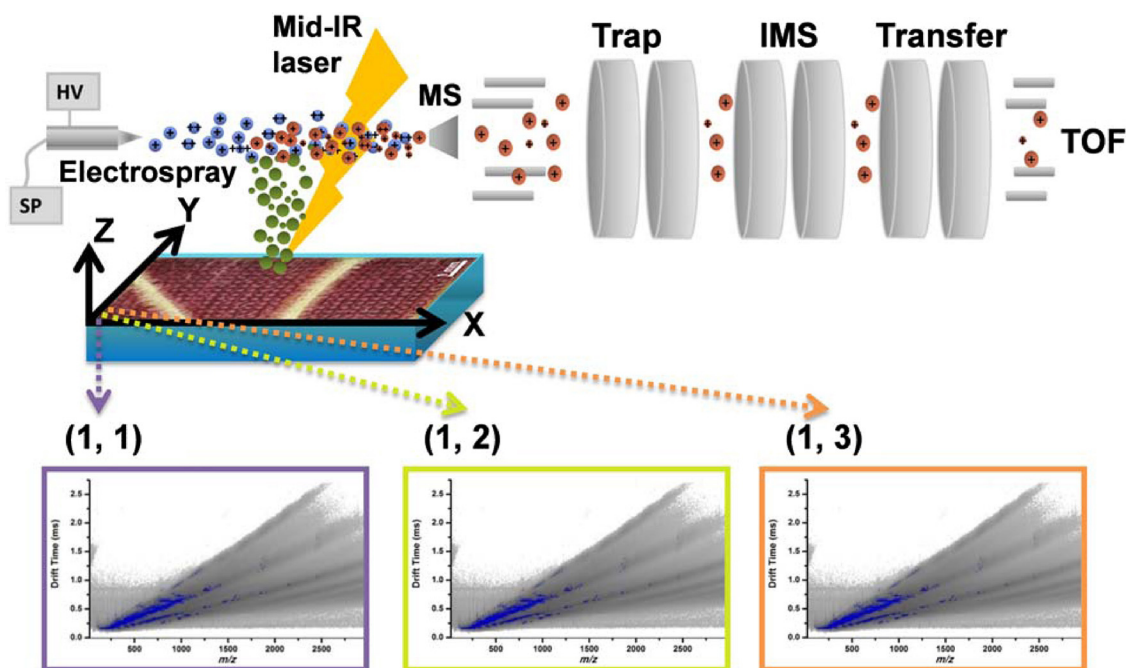


Fig. 1. Schematic of LAESI-IMS-MSI system, including laser ablation sampling, electrospray ionization, sample x - y positioning for surface mapping, traveling wave IMS, and time-of-flight MS. A DT vs. m/z plot is recorded and analyzed for each (x, y) position. Three examples of these plots are displayed for the (1, 1), (1, 2) and (1, 3) coordinates.

separation by interacting with the nitrogen buffer gas. Following separation, a traveling wave transfer tube, with adjustable collision energy, guided the ions into a Q-TOF analyzer. The three stage trap-IMS-transfer tube design enabled time aligned parallel (TAP) fragmentation by combining IMS with up to MS^3 for structure identification. Imaging experiments were conducted by rastering the biological sample under the focused laser beam in the x and y directions. Mass spectra were collected at each (x, y) position. Typically $250\ \mu\text{m}$ step sizes were selected for both the x and y direction. The number of laser pulses per position for a sample was determined by the average tissue thickness and laser energy. For example, a $60\ \mu\text{m}$ thick mouse brain tissue section required five laser pulses to ablate through. Defined by both the laser focal spot size and the selected step size, the lateral resolution of the LAESI-IMS-MSI system was demonstrated to be $180\ \mu\text{m}$. The schematic of LAESI-IMS-MSI is shown in Fig. 1.

Additional mouse brain tissue imaging experiments (the results are shown in Fig. 7) were conducted by a commercial LAESI system (DP-1000, Protea Biosciences, Morgantown, WV, USA) integrated with the IMS-MS instrument. The sampling event occurred at each predefined location on the tissue surface inside this system and the produced ions were analyzed by IMS-MS. The Peltier stage was kept at -10°C for the mouse brain tissue to significantly slow or arrest the metabolic activity. The system provides an

environmental chamber to control humidity in the vicinity of the sample. An average of five laser pulses were delivered at 10 Hz repetition rate to each preprogrammed spot on the mouse brain section. The time required for an imaging experiment depended on the size of the imaged area, the selected step sizes and the dwell time. A segment of the mouse brain tissue with dimensions of $9.5\ \text{mm} \times 5\ \text{mm}$ took approximately 1.1 h to image with $250\ \mu\text{m}$ step size (a total of 760 pixels) in a serpentine scanning mode.

2.2. Chemicals and samples

Water and methanol of HPLC grade were obtained from Alfa Aesar (Ward Hill, MA, USA). Glacial acetic acid was purchased from Fluka (Munich, Germany). All chemicals were used without further purification. A *Pelargonium peltatum* (cascading geranium) plant was secured from the Landscape Design Program of the George Washington University (Washington, DC, USA). Healthy *P. peltatum* leaves were analyzed immediately after removing them from the plant without further treatment. Mouse brain samples were obtained from a healthy BALB/c mouse strain provided by the Children's National Medical Center in accordance to Institutional Animal Use and Care Committee (IACUC) approvals. Mice were euthanized by cervical dislocation at average ages of 14 months. Brain specimens were snap-frozen using isopentane cooled in

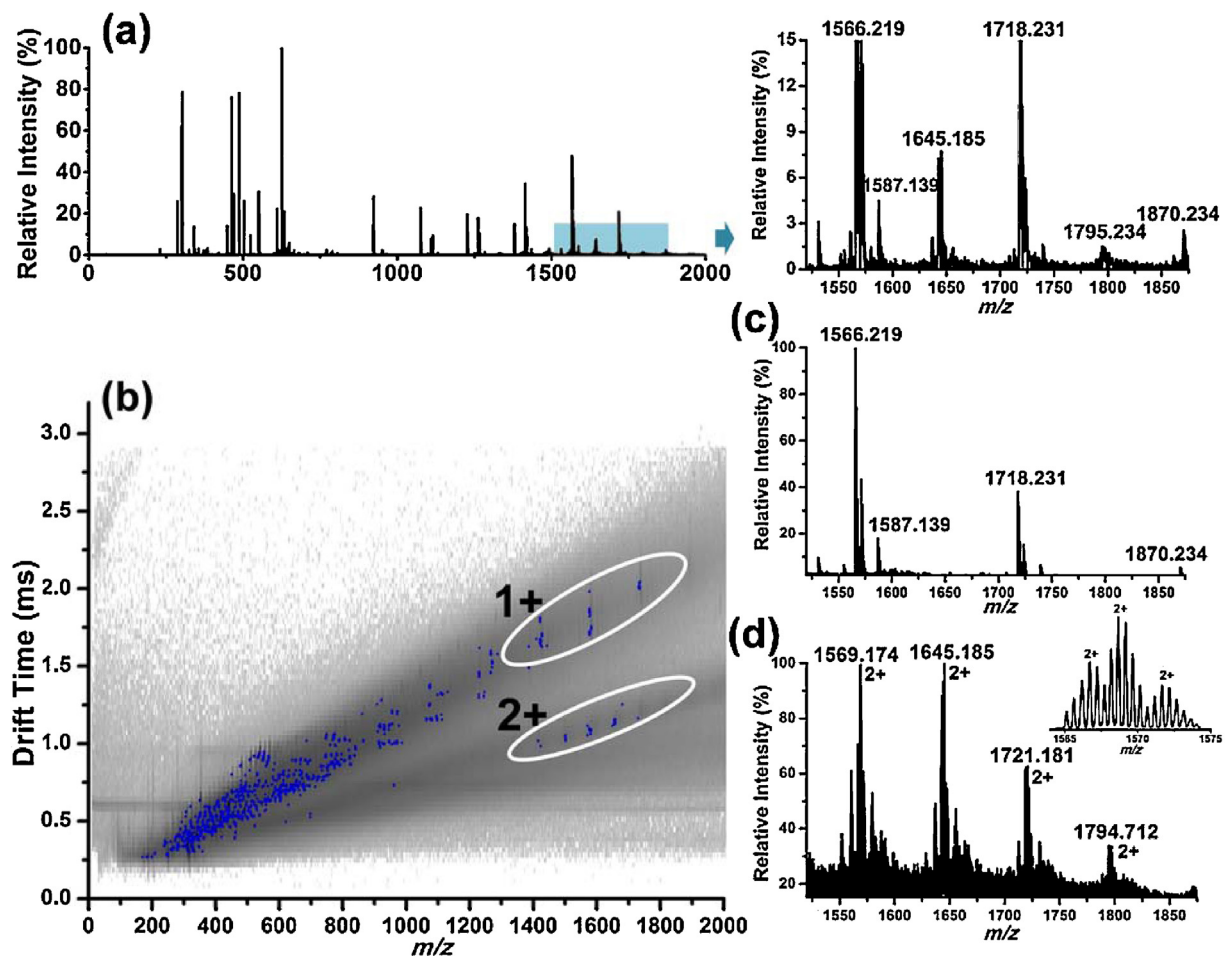


Fig. 2. Data associated with a pixel in a LAESI-IMS-MS imaging dataset for *P. peltatum* leaf. (a) Mass spectrum of the leaf tissue obtained by integrating the DT vs. m/z plot for all drift times. The zoomed version of the highlighted range between m/z 1500 and 1900 is displayed to the right. It exhibits interferences and the suppression of low intensity ions. (b) In the DT vs. m/z plot, the detected ions are marked by blue dots. Circled areas indicate the separation of singly and doubly charged ions from the m/z 1500–1900 range. (c) Extracting the mass spectrum from the selected singly charged ions results in significantly reduced interferences. (d) The mass spectrum corresponding to the selected doubly charged ions results in substantially enhanced signal-to-noise ratio due to reduced interferences and signal suppression.

liquid nitrogen and stored at -80°C . Sagittal sections ($60\ \mu\text{m}$) were prepared using a cryomicrotome (CM1900, LEICA Biosystems, Buffalo Grove, IL, USA) set to -25°C , mounted on microscope slides and stored at -80°C until further use.

2.3. Data processing

In a LAESI-IMS-MSI experiment, a multidimensional raw dataset composed of m/z and DT values, ion intensities, and pixel coordinates was collected. Fig. 1 shows three two-dimensional m/z vs. DT maps acquired at three different locations. It conveys the mass-to-charge ratios, charge states, and ion mobility values associated with the structural features of the detected ions. Mass spectra were examined and compared for different regions on the sample. Ions of interests were selected in the DT vs. m/z plots, and their intensities were rendered to express their distribution over the tissue surface. For the home-built LAESI system, a custom designed LabVIEW program was utilized to integrate ion intensities for each pixel. In case of electrospray emitter contamination, the experiment was halted, the emitter was cleaned and the corresponding scans were discarded. A scientific visualization package (Origin 8.5, OriginLab Northampton, MA, USA) was utilized to generate molecular distributions over the imaged area by representing ion intensities on a false-color scale.

For processing of the LAESI DP-1000 imaging datasets, ProteaPlot (version 2.0) software was utilized (see Fig. 7). The raw dataset was imported into ProteaPlot with a marker signal to correlate the scan numbers with the (x, y) positions on the surface. Averaged ion abundances at each location were represented by a false-color scale to reveal the spatial distribution of the selected ion. For isobaric species, datasets from the m/z vs. DT maps were exported for visualization by ProteaPlot.

3. Results and discussions

3.1. Molecular imaging of *P. peltatum* leaf

Initially, the abaxial surface of a *P. peltatum* leaf was imaged by the IMS-MSI system with the home-built LAESI source. To avoid artifacts from changes in tensile strength and water content, the region selected for imaging was a relatively small uniform portion of the *P. peltatum* leaf. Monitoring the detected total ion counts throughout the entire experiment showed less than a factor of two fluctuation, with no discernable trend (i.e., there was negligible drying).

Fig. 2(a) shows a mass spectrum, integrated over all DTs, corresponding to a single pixel in the image. The highlighted portion of the spectrum in the m/z 1500–1900 range is expanded to

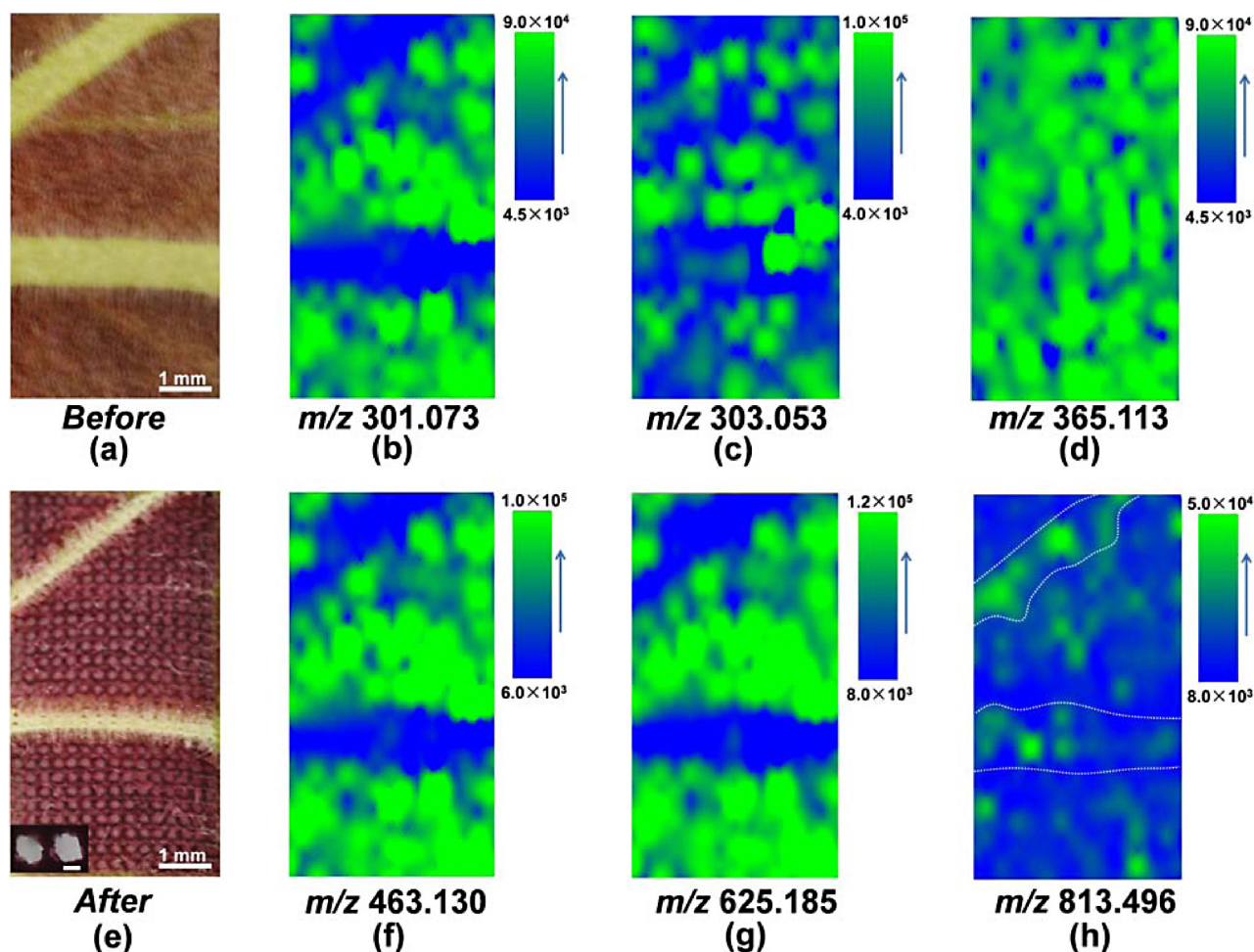


Fig. 3. Optical images (a) before and (e) after laser ablation sampling and ion distributions on the abaxial surface of *P. peltatum* leaf in a LAESI-IMS-MSI experiment. The inset in panel (e) shows two ablation marks in the tissue. Scale bar in the inset is $100\ \mu\text{m}$. Ion distributions correspond to (b) m/z 301.073, diosmetin, an O-methylated flavonoid, or its structural isomers, (c) m/z 303.053, quercetin or a structural isomer, (d) m/z 365.113, a disaccharide, (f) m/z 463.130, a glucoside of diosmetin or its structural isomers, (g) m/z 625.185, a diglucopyranosyl derivative of diosmetin or its structural isomers, and (h) m/z 813.496. Ions with m/z 301.073, 463.130 and 625.185 are absent in the vein region, whereas ions with m/z 303.053 and 365.113 exhibit a uniform distribution. The m/z 813.496 ion appears to have somewhat higher abundance in the vein region. The false color scale is based on the ion counts of the selected species.

show the presence of interfering peaks. In contrast the DT vs. m/z plot in Fig. 2(b) reveals the presence of singly and doubly charged ions in this m/z region clearly separated due to their different DTs. The mass spectra corresponding to the singly and doubly charged ions in the encircled areas are extracted and presented in Fig. 2(c) and (d), respectively. Based on tandem MS measurements (shown in Fig. S1), the singly charged and doubly charge ions in Fig. 2(c) are mixed clusters containing molecules with a mass of 152.01. Geraniol, an important component in the essential oils of plants in the *Pelargonium* genus, and many of its structural isomers have molecular weights close to this value [40,41]. The mass spectrum in Fig. 2(d) indicates a complex set of closely related ions. For example, the ion at m/z 1569.2 is surrounded by four satellite peaks at m/z 1552.2, 1560.7, 1579.7 and 1587.6. Furthermore, the isotope distribution pattern in the inset of Fig. 2(d) shows the presence of two additional species (m/z 1566.7 and 1571.7) adjacent to the ion with m/z 1569.2. None of these ions were discernable without IMS because the presence of these ions was obscured by the strong interfering peaks of the singly charged species and the low signal-to-noise ratio of the doubly charged ions. Overall, IMS improved the detection of ions with more peaks resolved, and expanded the molecular coverage in the tissue.

Fig. 3 shows optical and molecular images of the *P. peltatum* leaf tissue. The optical images in Fig. 3(a) before and Fig. 3(e) after the

analysis revealed the vein pattern in yellow color on the abaxial surface of the leaf. Laser ablation marks in the latter image show the locations of analysis on a rectangular grid. From the collected DT vs. m/z datasets, the intensities of selected ions were rendered to the points of analysis using false color scales (shown adjacent to the images) to represent the lateral distributions of the corresponding chemical species in the leaf.

As it is apparent from Fig. 3(b),(f) and (g) that depicts the distribution of ions m/z 301.073, 463.130 and 625.185, respectively, the corresponding chemical species exhibit high abundances in the purple areas of the leaf but are absent in the yellow colored vein regions. The accurate mass and the tandem MS (shown in Fig. S2 (a)) of m/z 301.073 indicate the presence of diosmetin, an O-methylated flavonoid, or its structural isomers [42]. Tandem MS of the ions with m/z 463.130 and 625.185 showed a fragment with m/z 301.072 that was close to the m/z 301.073 directly detected in the leaf spectra. The m/z differences between these three ions, shown in Fig. S2, identified m/z 463.130 as a glucoside and m/z 625.185 as a diglucopyranosyl derivative of the m/z 301.073 species.

However, Fig. 3(c) illustrates that the intensity of the ion with m/z 303.053, identified as quercetin or a structural isomer by tandem MS (shown in Fig. S2(b)), does not exhibit a correlation in its distribution with the pattern observed in the optical image.

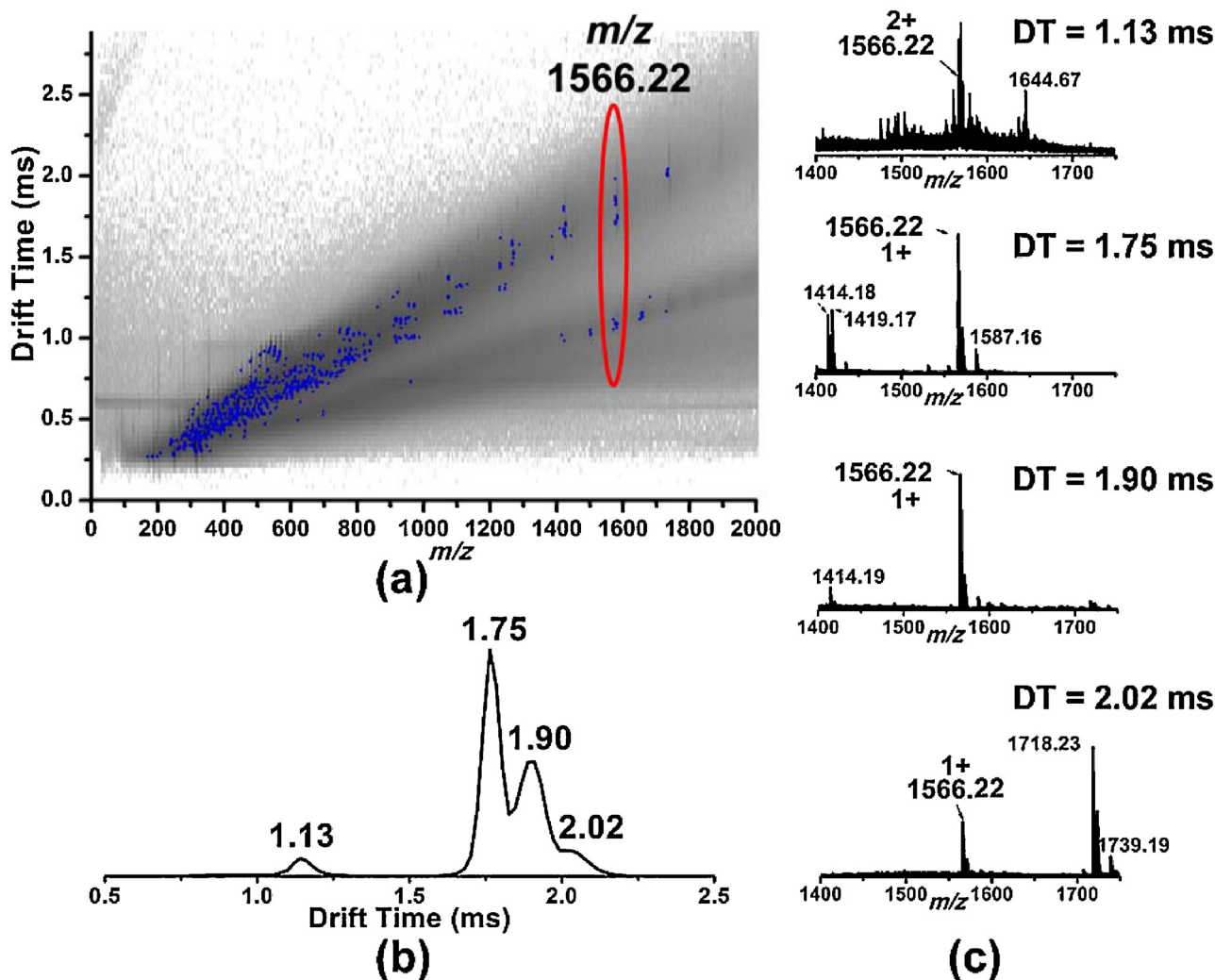


Fig. 4. Isobaric and close to isobaric ions can be distinguished by their DT in LAESI-IMS-MS. Panel (a) shows the DT vs. m/z plot corresponding to a single pixel in the molecular image of the *P. peltatum* leaf. In panel (b) the DT distribution for the ions with a window of 0.06 around m/z 1566.22 indicates the presence of four different species. Panel (c) shows the four mass spectra corresponding to the DTs identified in panel (b).

Similarly, in Fig. 3(d) the m/z 365.113, assigned as a sodiated disaccharide based on the tandem MS of the corresponding potassiumated species, the intensity distribution is uniform over the areas of different color. In contrast, Fig. 3(h) shows the distribution of the m/z 813.496 ion that appears to have somewhat higher abundance in the vein region.

In comparison to MALDI-IMS-MSI, the presented LAESI-IMS-MSI enables *in vivo* and *in situ* imaging with better coverage for small metabolites. However, the spatial resolution of MALDI-IMS-MSI in the tens of micrometers range compares favorably to the $\sim 180 \mu\text{m}$ resolution of LAESI-IMS-MSI.

3.2. Separation and imaging of isobaric ions

As a result of IMS, a number of isobaric ions, and ions with indistinguishable m/z due to the mass resolution limitations of the mass spectrometer were separated by their DTs in the spectra of the *P. peltatum* leaf. The DT vs. m/z plot in Fig. 4(a) indicates three isobaric and one close to isobaric ions at m/z 1566.22 exhibiting different DTs. The DT distribution selected for a 0.06 window around m/z 1566.22 in Fig. 4(b) shows that four DT peaks are present for this m/z and the mass spectra corresponding to the four DTs are shown in Fig. 4(c). The three peaks at 1.75, 1.90 and 2.02 ms in Fig. 4(b) correspond to singly charged isobaric ions indicating differences in collision cross sections due to the presence of structural isomers or conformers. The doubly charged ion at DT = 1.13 ms has a measured m/z of 1566.22 that, in the case of low level signal, in a mass spectrum without IMS cannot be distinguished from the other three ions.

To explore the nature of these species, tandem MS experiments were performed on the singly and doubly charged ions with m/z 1566.22 (see Fig. S1 in the Supporting information section). The

data indicates that protonated clusters of up to four molecules with a molecular mass of 152.01 (see peaks a–d in panels (c) and (d) of Fig. S1) are liberated from both the singly and doubly charged ions with m/z 1566.22. Peaks e and f in panel (c) and e–h and j in panel (d) correspond to mixed clusters containing molecules with a molecular mass of 152.01 and one or two other molecules.

Mass spectra in the vicinity of m/z 1566 in Fig 4(c) for the particular drift times indicate the presence of other ions with significantly lower and higher m/z . The ions at m/z 1414 exhibit the same DT = 1.75 ms as the singly charged m/z 1566 with the smallest collision cross section, whereas the ion with m/z 1739 has the same DT = 2.02 ms as the singly charged m/z 1566 with the largest collision cross section. This demonstrates that ions with significantly different m/z can have very similar collision cross sections.

The ability of IMS to distinguish isobaric and close to isobaric ions enabled imaging these species separately by LAESI-IMS-MS. Fig. 5 visualizes the distributions of close to isobaric species at m/z 1566 with DTs of 1.13 ms and 1.75 ms. The scales of both ion maps are normalized to the highest pixel ion count in the image. The doubly charged ion with DT = 1.13 ms shows a relatively uniform distribution throughout the studied area (see Fig. 5(a)), whereas the abundance of the singly charged ions with DT = 1.75 ms appears to be lower in the vein regions (see Fig. 5(b)). This example demonstrates that without IMS isobaric or close to isobaric ions can obscure the true nature of species distributions in MSI.

3.3. Imaging of mouse brain tissue section by LAESI-IMS-MS

Sagittal sections of frozen mouse brain tissue were mapped by LAESI-IMS-MSI. Fig. 6(a) shows the mass spectrum obtained by integrating the DT vs. m/z plot over all DTs for one pixel of the $60 \mu\text{m}$ thick tissue section. Molecules ranging from small

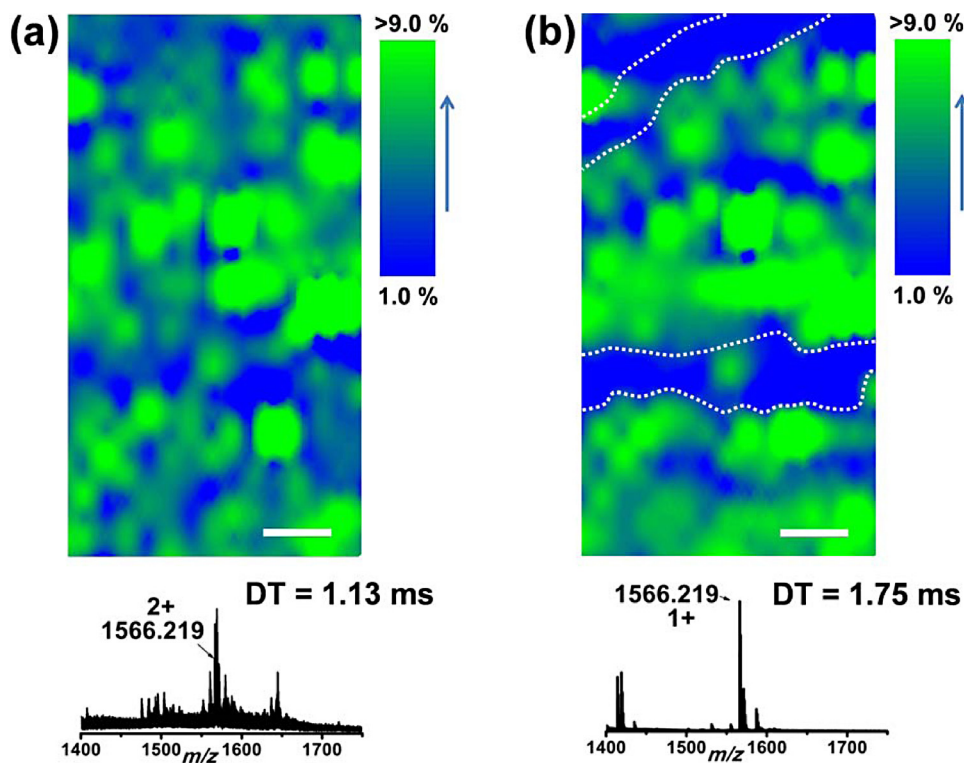


Fig. 5. Ion intensity distributions for two close to isobaric ions distinguished by IMS. Panel (a) presents the distribution for the doubly charged ion at m/z 1566.22 with DT = 1.13 ms, whereas in panel (b) the singly charged ion at m/z 1566.22 with DT = 1.75 ms is shown. The scale bar is 1 mm. The false color scale shows the ion count per pixel as a percentage of the brightest pixel in the image.

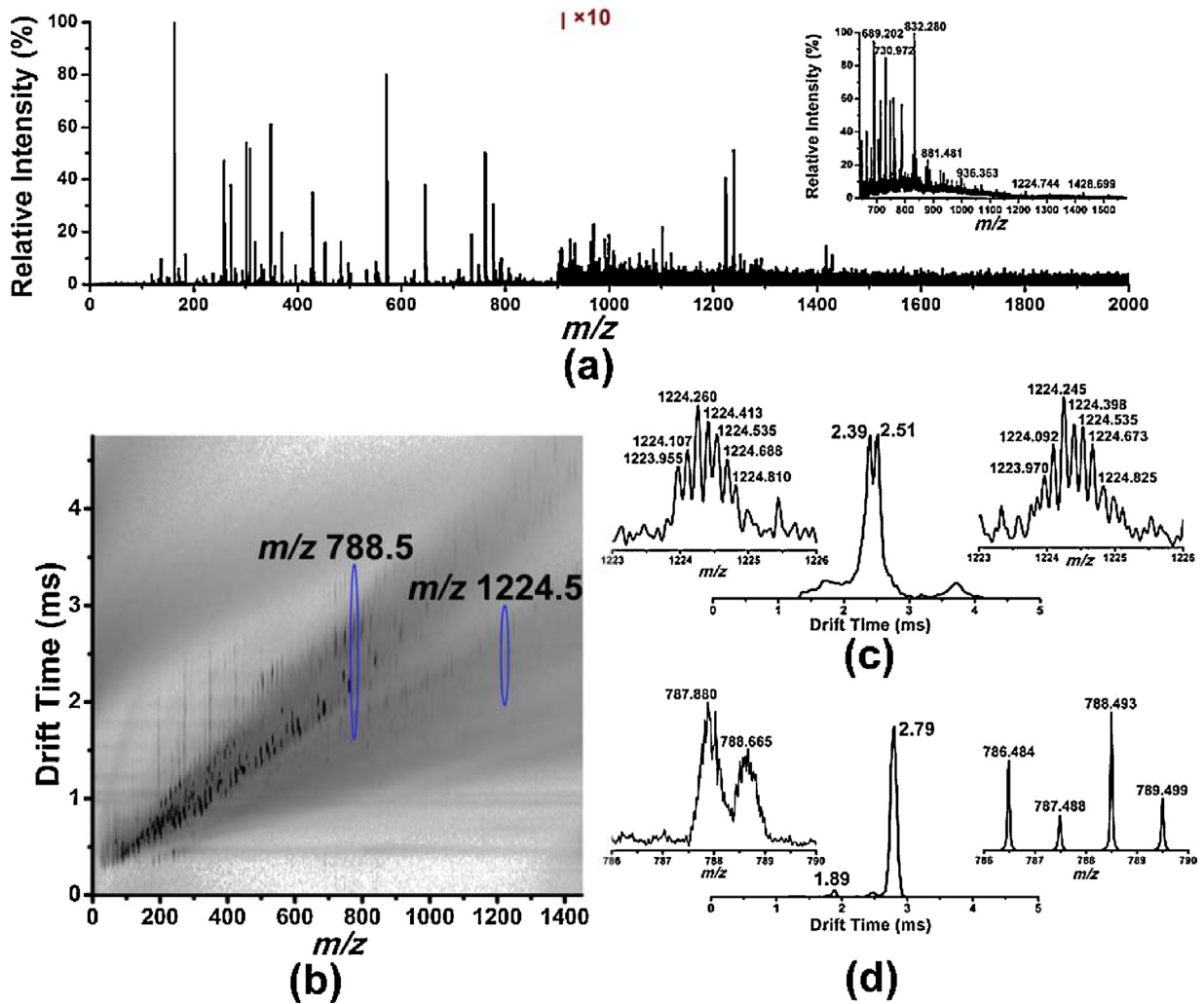


Fig. 6. Differentiation of isobaric ions in mouse brain tissue. (a) Mass spectrum of mouse brain tissue obtained by integrating for all DTs. The inset shows the multiply charged species of ~ 19 proteins. (b) DT vs. m/z plot for one pixel of mouse brain with two examples of isobaric ions at m/z 1224.53 and m/z 788.493. (c) Extracted DT distribution for the m/z 1224.53 ion reveal two peaks at DT = 2.39 and 2.51 ms. Corresponding insets show the mass spectra of polypeptides in their 7+ charge states. (d) Distribution of DT for the ions with $m/z \sim 788.5$ indicates the presence of two species at DT = 1.89 ms and 2.79 ms with very different intensities. Mass spectra extracted for the two DTs are shown in the insets.

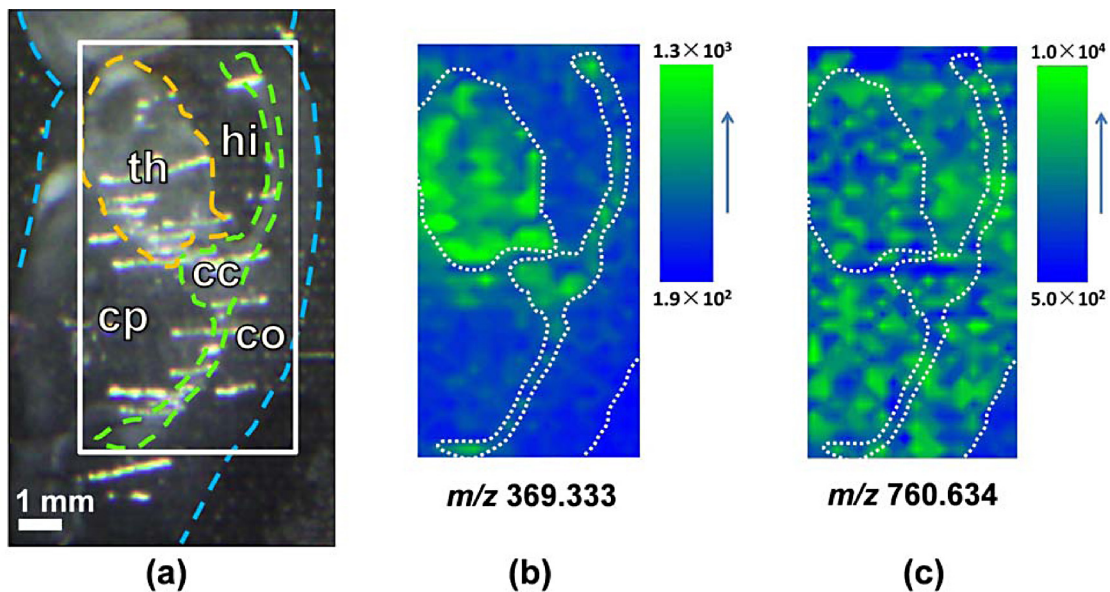


Fig. 7. (a) Optical image of sagittal mouse brain section with lines revealing anatomical regions of cortex (co), corpus callosum (cc), hippocampus (hi), thalamus (th) and caudate putamen (cp). Molecular distributions produced by LAESI-IMS-MSI for (b) $[M-H_2O+H]^+$ fragment of cholesterol show higher intensity in the thalamus and the corpus callosum, whereas for (c) m/z 760.634 (PC(34:1)) a uniform distribution is observed.

metabolites, through lipids and polypeptides to proteins were ionized and detected in the sample. The inset in Fig. 6(a) shows the multiply charged species of ~ 19 proteins. The majority of these protein ions were highly charged, typically with $z > 14$.

Fig. 6(b) shows that IMS helps to resolve the species with different conformations [38,43–45]. For example, the DT distribution for the m/z 1224.53 \pm 0.05 range exhibited two peaks at DT = 2.39 ms and 2.51 ms (see Fig. 6(c)). Selecting for these DT values revealed that the corresponding ions were in a charge state of $z = 7$, probably corresponding to polypeptides. The mass spectra in the insets of Fig. 6(c) indicate that the isotope distributions of these two isobaric or close to isobaric ions strongly resemble each other. Due to the relatively low intensity of this peak, the tandem MS spectra had insufficient resolution for identification. Furthermore, close to isobaric peaks with very different intensities (e.g., lipids and low abundance multiply charged proteins), that in a conventional mass spectrum leads to the suppression of the low intensity signal, were made distinguishable by IMS. Fig. 6(d) shows that close to isobaric ions selected in the m/z 788.493 \pm 0.02 range exhibit two distinct DT at 1.89 ms and 2.79 ms. The mass spectra extracted for the two DTs are shown in the insets of Fig. 6(d). Based on tandem MS, the four peaks in the right inset are identified as two lipid species and their isotope peaks. The signal in the left inset is weaker by a factor of 14 and it only becomes detectable as a result of IMS. Based on the spacing of the carbon isotope peaks these two species correspond to protein ions in the 20+ charge states.

A sagittal section of frozen mouse brain tissue was imaged by the LAESI DP-1000 integrated IMS–MSI system. The optical image in Fig. 7(a) reveals some anatomical features (cortex, corpus callosum, hippocampus, thalamus and caudate putamen) in the target area. In Fig. 7(b) the spatial distribution of the m/z 369.333 ion shows a higher intensity in the white matter, especially the corpus callosum and the thalamus regions, than in the grey matter. Based on earlier results the m/z 369.333 ion corresponds to the $[M-H_2O+H]^+$ fragment of cholesterol [46]. Our finding of higher abundance of cholesterol in the white matter is in agreement with previous literature reports [47–49]. In contrast, the m/z 760.634, identified in earlier studies as $[M+H]^+$ of PC(34:1) [46], displays a relatively uniform intensity distribution throughout the entire tissue section, a result that is consistent with previous studies performed by MALDI-MS [38].

4. Conclusions

Structural isomers with identical molecular weight often have dramatically different biological functions or clinical effects. Although in some cases tandem MS enables the differentiation of structural isomers, it often provides insufficient information for their identification by itself. The need for the distinction of structural isomers is exacerbated in direct ionization MS of biological samples without conventional extraction or separation steps. As a consequence, imaging by ambient ionization MS can produce molecular distributions that are distorted or obscured by such interferences.

The reported MSI technique is a synergistic combination of traveling wave IMS and LAESI–MSI with tandem MS ability incorporated. We demonstrated its advantages for mapping isobaric or close to isobaric biomolecules differentiated by their structures. Enhanced metabolite coverage has been achieved for direct imaging of untreated plant organs and animal tissue sections. Independent imaging of isobaric species sheds new light on the distributions of isomeric metabolites, lipids, polypeptides, and proteins with distinct molecular structures or conformations. The IMS–MSI of mouse brain tissue provided a new approach to mapping the distributions of isobaric compounds in frozen sections.

Acknowledgements

This material is based upon work supported by the U.S. National Science Foundation under Grant No. CHE-1152302, and the George Washington University Selective Excellence Fund.

Appendix A. Supplementary data

Supplementary data associated with this article can be found, in the online version, at <http://dx.doi.org/10.1016/j.ijms.2014.06.025>.

References

- [1] C. Wu, A.L. Dill, L.S. Eberlin, R.G. Cooks, D.R. Ifa, Mass spectrometry imaging under ambient conditions, *Mass Spectrom. Rev.* 32 (2013) 218–243.
- [2] A.L. Dill, L.S. Eberlin, D.R. Ifa, R.G. Cooks, Perspectives in imaging using mass spectrometry, *Chem. Commun.* 47 (2011) 2741–2746.
- [3] J.D. Watrous, T. Alexandrov, P.C. Dorrestein, The evolving field of imaging mass spectrometry and its impact on future biological research, *J. Mass Spectrom.* 46 (2011) 209–222.
- [4] E.R. Amstalden van Hove, D.F. Smith, R.M.A. Heeren, A concise review of mass spectrometry imaging, *J. Chromatogr. A* 1217 (2010) 3946–3954.
- [5] D. Miura, Y. Fujimura, H. Wariishi, In situ metabolomic mass spectrometry imaging: recent advances and difficulties, *J. Proteomics* 75 (2012) 5052–5060.
- [6] M. Wagner, Single-cell ecophysiology of microbes as revealed by Raman microspectroscopy or secondary ion mass spectrometry imaging, *Annu. Rev. Microbiol.* 63 (2009) 411–429.
- [7] R.M. Caprioli, T.B. Farmer, J. Gile, Molecular imaging of biological samples: localization of peptides and proteins using MALDI–TOF MS, *Anal. Chem.* 69 (1997) 4751–4760.
- [8] Y. Li, B. Shrestha, A. Vertes, Atmospheric pressure infrared MALDI imaging mass spectrometry for plant metabolomics, *Anal. Chem.* 80 (2008) 407–420.
- [9] J. Jurchen, S. Rubakhin, J. Sweedler, MALDI–MS imaging of features smaller than the size of the laser beam, *J. Am. Soc. Mass Spectrom.* 16 (2005) 1654–1659.
- [10] Z. Takáts, J.M. Wiseman, R.G. Cooks, Ambient mass spectrometry using desorption electrospray ionization (DESI): instrumentation, mechanisms and applications in forensics, chemistry, and biology, *J. Mass Spectrom.* 40 (2005) 1261–1275.
- [11] J.M. Wiseman, D.R. Ifa, Y. Zhu, C.B. Kissinger, N.E. Manicke, P.T. Kissinger, R.G. Cooks, Desorption electrospray ionization mass spectrometry: imaging drugs and metabolites in tissues, *Proc. Natl. Acad. Sci. U. S. A.* 105 (2008) 18120–18125.
- [12] C. Wu, D.R. Ifa, N.E. Manicke, R.G. Cooks, Molecular imaging of adrenal gland by desorption electrospray ionization mass spectrometry, *Analyst* 135 (2010) 28–32.
- [13] D.R. Ifa, C. Wu, Z. Ouyang, R.G. Cooks, Desorption electrospray ionization and other ambient ionization methods: current progress and preview, *Analyst* 135 (2010) 669–681.
- [14] P. Nemes, A. Vertes, Laser ablation electrospray ionization for atmospheric pressure, in vivo, and imaging mass spectrometry, *Anal. Chem.* 79 (2007) 8098–8106.
- [15] P. Nemes, A.A. Barton, Y. Li, A. Vertes, Ambient molecular imaging and depth profiling of live tissue by infrared laser ablation electrospray ionization mass spectrometry, *Anal. Chem.* 80 (2008) 4575–4582.
- [16] P. Nemes, A.A. Barton, A. Vertes, Three-dimensional imaging of metabolites in tissues under ambient conditions by laser ablation electrospray ionization mass spectrometry, *Anal. Chem.* 81 (2009) 6668–6675.
- [17] A. Vaikinen, T. Kotiaho, R. Kostianen, T.J. Kauppila, Desorption atmospheric pressure photoionization with polydimethylsiloxane as extraction phase and sample plate material, *Anal. Chim. Acta* 682 (2010) 1–8.
- [18] K. Hiraoka, K. Nishidate, K. Mori, D. Asakawa, S. Suzuki, Development of probe electrospray using a solid needle, *Rapid Commun. Mass Spectrom.* 21 (2007) 3139–3144.
- [19] P.J. Roach, J. Laskin, A. Laskin, Nanospray desorption electrospray ionization: an ambient method for liquid-extraction surface sampling in mass spectrometry, *Analyst* 135 (2010) 2233–2236.
- [20] I. Lanekoff, O. Geydebekht, G.E. Pinchuk, A.E. Konopka, J. Laskin, Spatially resolved analysis of glycolipids and metabolites in living *Synechococcus* sp. PCC 7002 using nanospray desorption electrospray ionization, *Analyst* 138 (2013) 1971–1978.
- [21] P. Nemes, H. Huang, A. Vertes, Internal energy deposition and ion fragmentation in atmospheric-pressure mid-infrared laser ablation electrospray ionization, *Phys. Chem. Chem. Phys.* 14 (2012) 2501–2507.
- [22] S.S. Rubakhin, J.C. Jurchen, E.B. Monroe, J.V. Sweedler, Imaging mass spectrometry: fundamentals and applications to drug discovery, *Drug Discov. Today* 10 (2005) 823–837.
- [23] D.R. Ifa, L.M. Gumaelius, L.S. Eberlin, N.E. Manicke, R.G. Cooks, Forensic analysis of inks by imaging desorption electrospray ionization (DESI) mass spectrometry, *Analyst* 132 (2007) 461–467.

- [24] Z. Chen, A. Bogaerts, A. Vertes, Phase explosion in atmospheric pressure infrared laser ablation from water-rich targets, *Appl. Phys. Lett.* 89 (2006) 041503.
- [25] Z.Y. Chen, A. Vertes, Early plume expansion in atmospheric pressure midinfrared laser ablation of water-rich targets, *Phys. Rev. E* 77 (2008) 036316.
- [26] A. Vertes, P. Nemes, B. Shrestha, A. Barton, Z. Chen, Y. Li, Molecular imaging by Mid-IR laser ablation mass spectrometry, *Appl. Phys. A* 93 (2008) 885–891.
- [27] R.M.A. Heeren, D.F. Smith, J. Stauber, B. Kükrer-Kaletas, L. MacAleese, Imaging mass spectrometry: hype or hope? *J. Am. Soc. Mass Spectrom.* 20 (2009) 1006–1014.
- [28] A.S. Woods, M. Ugarov, T. Egan, J. Koomen, K.J. Gillig, K. Fuhrer, M. Gonin, J.A. Schultz, Lipid/peptide/nucleotide separation with MALDI-Ion Mobility-TOF MS, *Anal. Chem.* 76 (2004) 2187–2195.
- [29] J.A. McLean, B.T. Ruotolo, K.J. Gillig, D.H. Russell, Ion mobility mass spectrometry: a new paradigm for proteomics, *Int. J. Mass Spectrom.* 240 (2005) 301–315.
- [30] M.J. Cohen, F.W. Karasek, Plasma chromatography – a new dimension for gas chromatography and mass spectrometry, *J. Chromatogr. Sci.* 8 (1970) 330–337.
- [31] D.E. Clemmer, M.F. Jarrold, Ion mobility measurements and their applications to clusters and biomolecules, *J. Mass Spectrom.* 32 (1997) 577–592.
- [32] J.A. McLean, W.B. Ridenour, R.M. Caprioli, Profiling and imaging of tissues by imaging ion mobility-mass spectrometry, *J. Mass Spectrom.* 42 (2007) 1099–1105.
- [33] E.Q. Blatherwick, C.I. Svensson, B.G. Frenguelli, J.H. Scrivens, Localisation of adenine nucleotides in heat-stabilised mouse brains using ion mobility enabled MALDI imaging, *Int. J. Mass Spectrom.* 345–347 (2013) 19–27.
- [34] P.J. Trim, C.M. Henson, J.L. Avery, A. McEwen, M.F. Snel, E. Claude, P.S. Marshall, A. West, A.P. Princivalle, M.R. Clench, Matrix-assisted laser desorption/ionization-ion mobility separation-mass spectrometry imaging of vinblastine in whole body tissue sections, *Anal. Chem.* 80 (2008) 8628–8634.
- [35] J. Stauber, L. MacAleese, J. Franck, E. Claude, M. Snel, B.K. Kaletas, I.M.V.D. Wiel, M. Wisztorski, I. Fournier, R.M.A. Heeren, On-tissue protein identification and imaging by MALDI-ion mobility mass spectrometry, *J. Am. Soc. Mass Spectrom.* 21 (2010) 338–347.
- [36] M. Kliman, J.C. May, J.A. McLean, Lipid analysis and lipidomics by structurally selective ion mobility-mass spectrometry, *Biochim. Biophys. Acta* 1811 (2011) 935–945.
- [37] L.M. Cole, K. Mahmoud, S. Haywood-Small, G.M. Tozer, D.P. Smith, M.R. Clench, Recombinant "IMS TAG" proteins – a new method for validating bottom-up matrix-assisted laser desorption/ionisation ion mobility separation mass spectrometry imaging, *Rapid Commun. Mass Spectrom.* 27 (2013) 2355–2362.
- [38] S.N. Jackson, M. Ugarov, T. Egan, J.D. Post, D. Langlais, J. Albert Schultz, A.S. Woods, MALDI-ion mobility-TOFMS imaging of lipids in rat brain tissue, *J. Mass Spectrom.* 42 (2007) 1093–1098.
- [39] S. Trimpin, T.N. Herath, E.D. Inutan, J. Wager-Miller, P. Kowalski, E. Claude, J.M. Walker, K. Mackie, Automated solvent-free matrix deposition for tissue imaging by mass spectrometry, *Anal. Chem.* 82 (2009) 359–367.
- [40] R.A. Shellie, P.J. Marriott, Comprehensive two-dimensional gas chromatography-mass spectrometry analysis of Pelargonium graveolens essential oil using rapid scanning quadrupole mass spectrometry, *Analyst* 128 (2003) 879–883.
- [41] M. Lorenzo Tejedor, H. Mizuno, N. Tsuyama, T. Harada, T. Masujima, In situ molecular analysis of plant tissues by live single-cell mass spectrometry, *Anal. Chem.* 84 (2011) 5221–5228.
- [42] L. Silvestro, I. Tarcomnicu, C. Dulea, N. Attili, V. Ciuca, D. Peru, S.R. Savu, Confirmation of diosmetin 3-O-glucuronide as major metabolite of diosmin in humans, using micro-liquid-chromatography-mass spectrometry and ion mobility mass spectrometry, *Anal. Bioanal. Chem.* 405 (2013) 8295–8310.
- [43] S.D. Pringle, K. Giles, J.L. Wildgoose, J.P. Williams, S.E. Slade, K. Thalassinou, R.H. Bateman, M.T. Bowers, J.H. Scrivens, An investigation of the mobility separation of some peptide and protein ions using a new hybrid quadrupole/travelling wave IMS/oa-ToF instrument, *Int. J. Mass Spectrom.* 261 (2007) 1–12.
- [44] A.B. Kanu, P. Dwivedi, M. Tam, L. Matz, H.H. Hill, Ion mobility-mass spectrometry, *J. Mass Spectrom.* 43 (2008) 1–22.
- [45] B. Shrestha, A. Vertes, High-throughput cell and tissue analysis with enhanced molecular coverage by laser ablation electrospray ionization mass spectrometry using ion mobility separation, *Anal. Chem.* 86 (2014) 4308–4315.
- [46] B. Shrestha, P. Nemes, J. Nazarian, Y. Hathout, E.P. Hoffman, A. Vertes, Direct analysis of lipids and small metabolites in mouse brain tissue by AP IR-MALDI and reactive LAESI mass spectrometry, *Analyst* 135 (2010) 751–758.
- [47] C. Wu, D.R. Ifa, N.E. Manicke, R.G. Cooks, Rapid, direct analysis of cholesterol by charge labeling in reactive desorption electrospray ionization, *Anal. Chem.* 81 (2009) 7618–7624.
- [48] D. Touboul, F. Halgand, A. Brunelle, R. Kersting, E. Tallarek, B. Hagenhoff, O. Laprevote, Tissue molecular ion imaging by gold cluster ion bombardment, *Anal. Chem.* 76 (2004) 1550–1559.
- [49] P. Sjövall, B. Johansson, J. Lausmaa, Localization of lipids in freeze-dried mouse brain sections by imaging TOF-SIMS, *Appl. Surf. Sci.* 252 (2006) 6966–6974.

Supporting information for

**Ambient Molecular Imaging by Laser Ablation
Electrospray Ionization Mass Spectrometry with
Ion Mobility Separation**

*Hang Li,¹ Brian K. Smith,¹ László Márk,² Peter Nemes,¹ Javad Nazarian^{3,4} and Akos Vertes*¹*

¹Department of Chemistry, W. M. Keck Institute for Proteomics Technology and Applications,
The George Washington University, Washington, DC 20052, USA

²Department of Analytical Biochemistry, Institute of Biochemistry and Medical Chemistry,
Janos Szentagothai Research Center, MTA-PTE Human Reproductive Research Group,
University of Pécs, H-7624 Pécs, Hungary

³Research Center for Genetic Medicine, Children's National Medical Center, Washington, DC
20010, USA

⁴Department of Integrative Systems Biology, The George Washington University, School of
Medicine and Health Sciences, Washington, DC 20052, USA

***Corresponding Author:** Tel.: +1 (202) 994-2717; fax: +1 (202) 994-5873. E-mail address:
vertes@gwu.edu (A. Vertes). Address: Department of Chemistry, The George Washington
University, 725 21-st Street, N.W., Washington, DC 20052, USA.

Fig. S1. Tandem mass spectra and drift time (DT) distributions of the isobaric ions at m/z 1566.22 in *P. peltatum* leaf. Panel (a) and (b) are the DT distributions for m/z 1566.22 in MS and tandem MS mode, respectively. The shorter DT at ~ 1.5 ms represents the doubly charged ions, whereas the longer DT at ~ 2.5 ms represents the singly charged ions. Panels (c) and (d) are tandem mass spectra for singly charged and doubly charged m/z 1566.22, respectively. In panel (c), the mass differences between peaks a and b, b and c, c and d, and e and f are 152.02 ± 0.01 . In panel (d), the mass differences between a and b, b and c, c and d, e and f, f and g, g and h, and i and j are 152.01 ± 0.01 . This data indicates that protonated clusters of up to four molecules with a molecular mass of 152.01 (see peaks a, b, c, and d) are liberated from both the singly and doubly charged ion with m/z 1566.22. Peaks e and f in panel (c) and e, f, g, h and j in panel (d) correspond to mixed clusters containing molecules with a molecular mass of 152.01 and one or two other molecules.

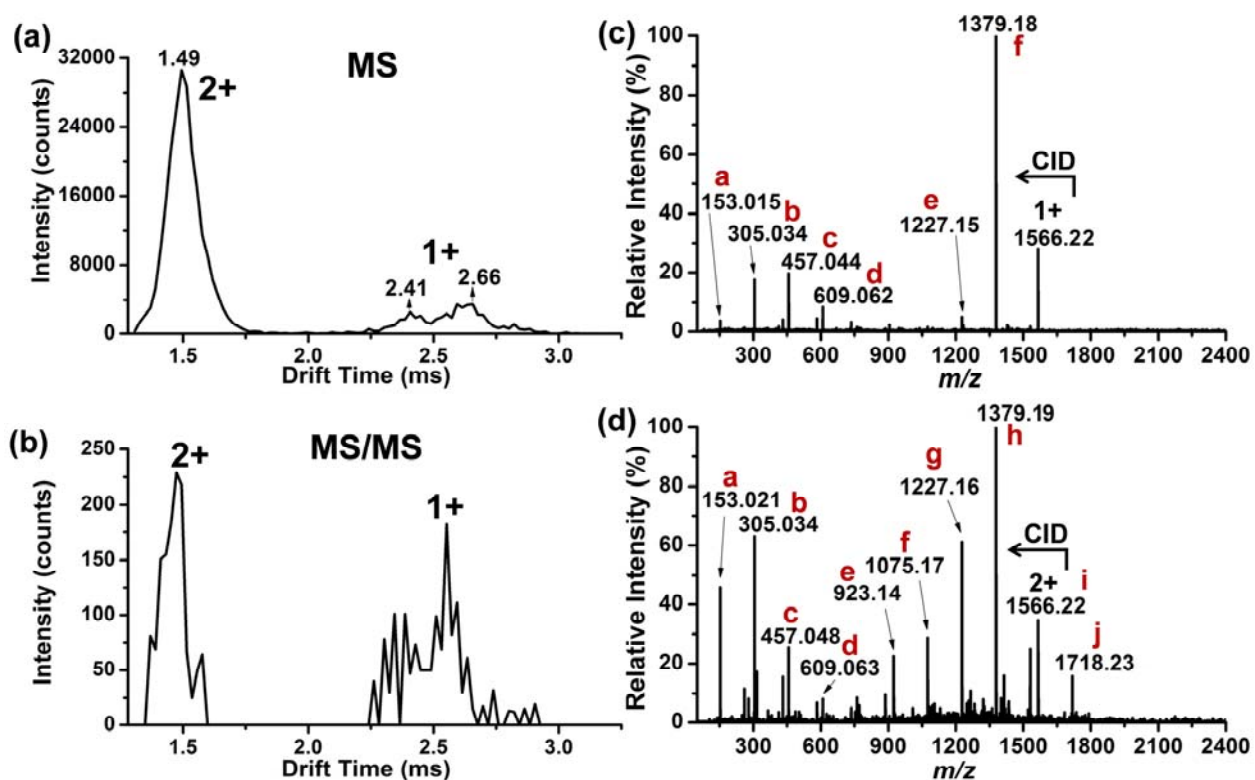


Fig. S2. Examples of tandem mass spectra used in conjunction with database information for metabolite assignments: (a) diosmetin at m/z 301.074, (b) quercetin at m/z 303.052, (c) disaccharide at m/z 365.104 (d) diosmetin-glucoside at m/z 463.135, (e) di-C-glucopyranosyldiosmetin at m/z 625.177.

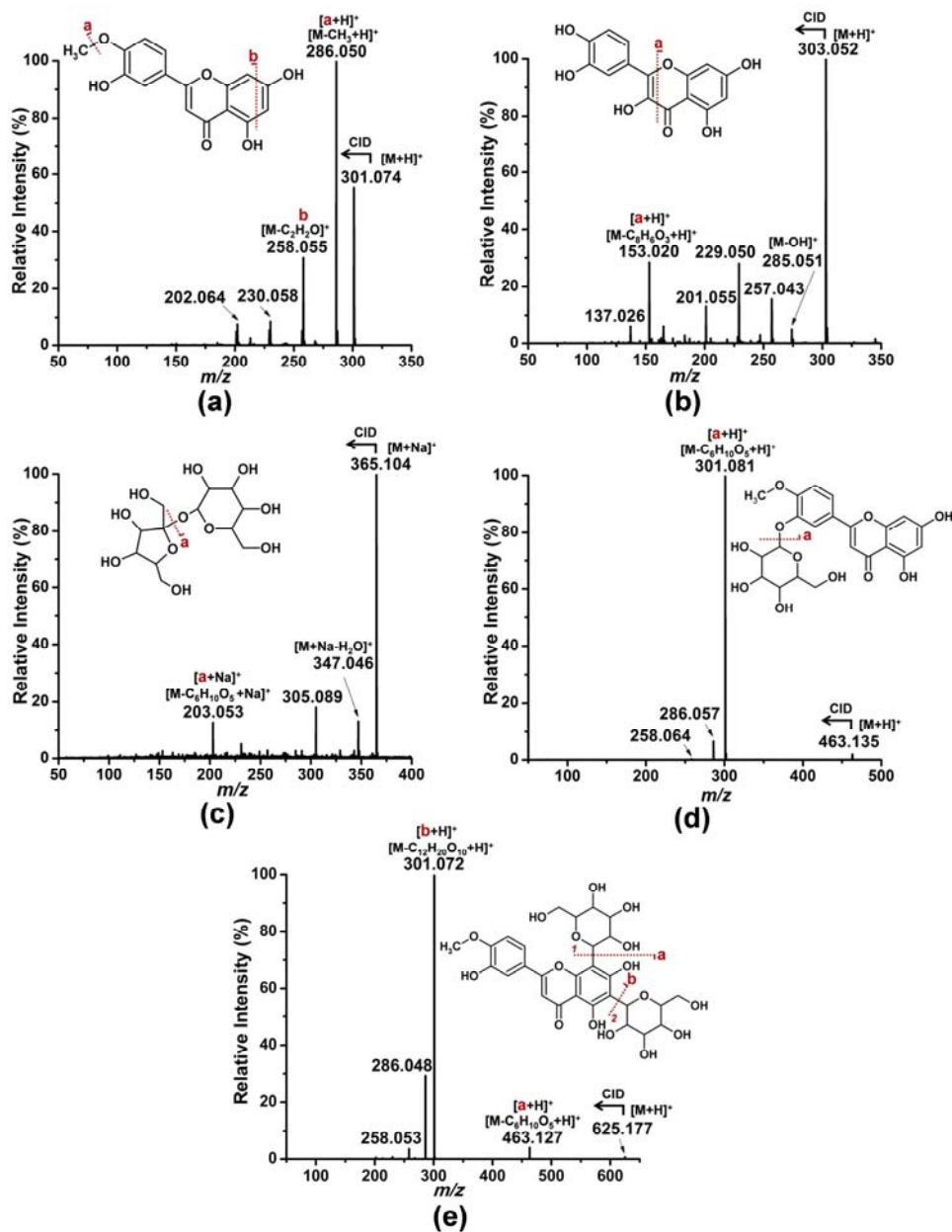


Table S1. Tentative peak assignments for positive ions in LAESI-MS of *P. peltatum* leaf based on accurate mass measurement, isotope pattern comparison, tandem MS, and database search (PlantCyc, <http://www.plantcyc.org/>, LIPID MAPS, <http://www.lipidmaps.org/>, and METLIN, <http://metlin.scripps.edu/>).

Chemical Name	Chemical Formula		Measured <i>m/z</i>	Monoisotopic mass	Δm (mDa)
oxomalonate	C ₃ H ₂ O ₅	[M+H] ⁺	119.003	118.9980	5.0
monosaccharide	C ₆ H ₁₂ O ₆	[M+K] ⁺	219.023	219.0271	-4.1
gamma-glutaminyloxybenzene	C ₁₁ H ₁₄ N ₂ O ₄	[M+Na] ⁺	261.082	261.0851	-3.1
hydroxyflavanone	C ₁₅ H ₁₂ O ₃	[M+Na] ⁺	263.066	263.0684	-2.4
kaempferol, luteolin ^a	C ₁₅ H ₁₀ O ₆	[M+H] ⁺	287.055	287.0556	-0.6
diosmetin ^a	C ₁₆ H ₁₂ O ₆	[M+H] ⁺	301.073	301.0712	1.8
quercetin ^a	C ₁₅ H ₁₀ O ₇	[M+H] ⁺	303.053	303.0505	2.5
acetylkaempferol, acetylluteolin	C ₁₇ H ₁₂ O ₇	[M+H] ⁺	329.062	329.0661	-4.1
disaccharide ^a	C ₁₂ H ₂₂ O ₁₁	[M+Na] ⁺ [M+K] ⁺	365.113 381.084	365.1060 381.0799	7.0 4.1
di-O-methylquercetin	C ₁₇ H ₁₄ O ₇	[M+K] ⁺	369.046	369.0377	8.3
hydroxy-methoxymethylenedioxyflavanone	C ₁₉ H ₁₄ O ₇	[M+Na] ⁺	377.064	377.0637	0.3
diosmetin glucoside ^a	C ₂₂ H ₂₂ O ₁₁	[M+H] ⁺	463.130	463.1240	6.0
glycitein-O-glucuronide	C ₂₂ H ₂₀ O ₁₁	[M+Na] ⁺	483.084	483.0903	-6.3
kaempferol-galactoside ^a	C ₂₁ H ₂₀ O ₁₁	[M+K] ⁺	487.074	487.0643	9.7
quercetagenin-glucoside ^a	C ₂₁ H ₂₀ O ₁₃	[M+Na] ⁺	503.071	503.0802	-9.2
di-C-glucopyranosyldiosmetin ^a	C ₂₈ H ₃₂ O ₁₆	[M+H] ⁺	625.185	625.1769	8.1
quercetin-galloylglucoside ^a	C ₂₈ H ₂₄ O ₁₆	[M+Na] ⁺	639.097	639.0962	0.8

^aTandem MS was performed for chemical species assignment.